Journal of Catalysis 286 (2012) 51–61

Contents lists available at SciVerse ScienceDirect

Journal of Catalysis

journal homepage: www.elsevier.com/locate/jcat

Structure and catalytic performance of alumina-supported copper–cobalt catalysts for carbon monoxide hydrogenation

Jingjuan Wang [a,b], Petr A. Chernavskii [c], Andrei Y. Khodakov [b,*], Ye Wang [a]

[a] State Key Laboratory of Physical Chemistry of Solid Surfaces, National Engineering Laboratory for Green Chemical Productions of Alcohols, Ethers and Esters, College of Chemistry and Chemical Engineering, Xiamen University, Xiamen 361005, China
[b] Unité de Catalyse et de Chimie du Solide, UMR 8181 CNRS, Bât. C3, USTL-ENSCL-EC Lille, Cité Scientique, 59655 Villeneuve d'Ascq, France
[c] Department of Chemistry, Moscow State University, 119992 Moscow, Russia

ARTICLE INFO

Article history:
Received 2 May 2011
Revised 11 October 2011
Accepted 16 October 2011
Available online 20 November 2011

Keywords:
Co–Cu catalysts
Higher alcohols synthesis
Syngas conversion
In situ characterization

ABSTRACT

The structure of alumina-supported copper–cobalt catalysts prepared by incipient co-impregnation was studied by using a combination of various characterization techniques including *in situ* XRD, XPS, TPR, XANES/EXAFS, *in situ* magnetic method, and TEM. The results suggest a much higher dispersion of copper than cobalt on γ-Al_2O_3 and a stronger interaction between cobalt and copper oxide particles, leading to the formation of mixed copper–cobalt oxides in the calcined catalysts. Cobalt reduction was significantly enhanced in the presence of copper. Furthermore, our characterizations indicate the formation of bimetallic Cu–Co particles in the reduced catalysts and enrichment of the surface of bimetallic particles with Cu. The catalytic studies showed dramatic modifications of both the rate and selectivity in the hydrogenation of CO after addition of even small amounts of Cu to supported Co catalysts. The presence of Cu increased the selectivity to alcohols by an order of magnitude and decreased the overall carbon monoxide conversion. Structure-performance correlations suggest that the Cu–Co bimetallic particles may be involved in higher alcohol synthesis.

1. Introduction

The catalytic conversion of syngas derived from natural gas, coal, and biomass to valuable long-chain hydrocarbons and alcohols is one of the challenging and attractive subjects in the field of C1 chemistry [1–3]. The hydrocarbons and alcohols obtained from this process can be used as fuels, fuel additives for octane or cetane enhancement, and intermediates for value-added chemicals such as medicine, cosmetics, and polyester. The major challenge of carbon monoxide hydrogenation is the efficient control of the reaction selectivity to olefins, long-chain paraffins, or oxygenated products. Cobalt catalysts are the catalysts of choice for synthesis of long-chain paraffins using Fischer–Tropsch reaction, while copper-containing catalysts are selective in methanol synthesis from syngas. Both cobalt and copper catalysts are currently used in relevant large-scale industrial processes. It could be therefore expected that mixed copper–cobalt catalysts would have higher selectivity to C2+ alcohols.

It is known that the promotion of cobalt catalysts with different metals could lead to higher Fischer–Tropsch reaction rates and could also affect selectivity. The modifications of catalyst structure and catalytic performance that are due to the promotion with the noble metals (Ru, Pt, Re, Pd) have been addressed in several reports [4–7]. The amount of promoting noble metal is usually very low, because of higher prices and rarity of these metals and sometimes their detrimental effects on the selectivity to long-chain hydrocarbons (e.g., Pt [4]). Recently, it was found [8,9] that addition of small amounts of Mn can enhance selectivity to higher hydrocarbons in Fischer–Tropsch synthesis. Promotion with Mn of carbon nanofibres and silica-supported catalysts resulted in higher C5+ selectivity that was accompanied with some smaller decrease in carbon monoxide conversion rate. The observed increase in C5+-selectivity for higher MnO loadings was attributed to the increase in the CH_x coverage measured from SSITKA experiments [9].

Several attempts have been made in the past to design a viable industrial process for synthesis of higher alcohols from $H_2/CO/CO_2$ mixtures (e.g., isobutanol synthesis, Synol process [10]). All these attempts, however, have not resulted in any major industrial manufacturing. The major difficulties include catalyst deactivation, low alcohol productivity, insufficient selectivity, and very complex mixture of reaction products [11,12].

Catalytic systems based on rhodium, copper–zinc, molybdenum oxide, sulfide-based catalysts, and copper–cobalt precipitated catalysts have been investigated for higher alcohol synthesis [1,2,11]. Rhodium-based catalysts have shown so far the best selectivity for

* Corresponding author.
E-mail address: andrei.khodakov@univ-lille1.fr (A.Y. Khodakov).

0021-9517/$ - see front matter © 2011 Elsevier Inc. All rights reserved.
doi:10.1016/j.jcat.2011.10.012

higher alcohol synthesis [1,13–17]. However, the limited availability and high price of rhodium restrict industrial application of these catalysts. Several recent reviews have addressed modified copper–zinc methanol synthesis catalysts and molybdenum-based catalysts for the higher alcohol synthesis [1–3].

It is expected that the efficient control of selectivity either to hydrocarbons or to oxygenates may be achieved by using supported bimetallic cobalt–copper catalysts. The copper–cobalt catalysts for higher alcohol synthesis were first designed in 1970s in the IFP [18]. A large number of patent applications and papers, which focused on promoted Co–Cu-based catalysts for higher alcohol synthesis from syngas, appeared afterward [1,19–23]. The catalysts were typically prepared by either coprecipitation of metal nitrates with alkali carbonates or by pyrolysis, in which an organic acid, such as citric acid [24], was added to the mixture of metal nitrates before calcination [25]. Most of the catalyst preparation details have not been, however, disclosed in the open literature. In addition, several authors [26,27] have reported difficult reproducibility of the synthesis of copper–cobalt catalysts via coprecipitation or pyrolysis. Indeed, all preparation steps in the catalyst syntheses should be controlled with a great efficiency to obtain high and reproducible alcohol productivities.

Two major concepts about the nature of the active sites in copper–cobalt catalysts for higher alcohol synthesis have been developed. First, it has been suggested that the formation of higher alcohols may involve CuCo bimetallic sites [18,28,29]. Second, the formation of alcohols has been attributed to a synergy between metallic copper and partially reduced cobalt species [30–33]. To provide further insights into the active sites for alcohol synthesis, Subramanian et al. [34] investigated unsupported Cu–Co mixed nanoparticle model catalysts for alcohol synthesis from syngas and found that the Cu–Co mixed nanoparticles were more selective to ethanol than core–shell structured counterparts containing Co-core and Cu-shell. Though unsupported nanoparticles seem to be a good model system to study the active sites and mechanisms of carbon monoxide hydrogenation, the catalyst handling (e.g., pyrophoricity) and catalyst stability are problematic for long-term and large-scale operations. Insufficient stability is also one of the major problems relevant to the industrial use of the precipitated copper–cobalt catalysts [35].

It has been demonstrated recently that porous structure of the support may efficiently control the metal dispersion [36–39]. In the catalysts supported by porous oxides, the sizes of metal particles are typically limited by pore sizes of the support [39,40]. In contrast to the catalysts prepared by coprecipitation, in supported catalysts, the support texture may prevent sintering of metal particles [39,40] or limit sintering to the maximum pore diameter [41,42]. The support (e.g., alumina) can also strengthen the mechanical stability of a catalyst, which is particularly important for fluidized bed and slurry bubble column applications. However, it can be expected that the interactions between copper and cobalt might be different in the supported catalysts compared to the catalysts prepared by coprecipitation, which may lead to different structure of active phases and different catalytic performances.

In this paper, a series of alumina-supported Cu–Co catalysts are prepared by incipient wetness impregnation and are characterized by a wide range of spectroscopic techniques. Higher copper contents are used in this work in contrast to the cobalt catalysts promoted with noble metals. The catalytic performances of the promoted catalysts in carbon monoxide hydrogenation are examined in a fixed bed microreactor. The correlations between the catalyst structure and catalytic performance are discussed to gain insights into the probable active sites for the hydrogenation of carbon monoxide over the bimetallic catalysts.

2. Experimental

2.1. Catalyst preparation

Commercial γ-Al_2O_3 (Puralox SCCA 5/170 from Sasol, Germany) with BET surface areas of $\sim$165 $m^2\,g^{-1}$, pore volume of 0.47 $cm^3\,g^{-1}$, and pore diameter of 8 nm was used as support. The monometallic and bimetallic Cu–Co catalysts were prepared by incipient wetness co-impregnation of γ-Al_2O_3 using aqueous solutions of cobalt nitrate or copper nitrate. Co-impregnation was used instead of sequential impregnation, because it might provide better alcohol yields [43]. Aqueous solution of $Co(NO_3)_2{\cdot}6H_2O$ and/or $Cu(NO_3)_2{\cdot}3H_2O$ was added dropwise into dry alumina powder with continuous stirring; the samples were aged at room temperature for about 4 h. The catalysts with 20 wt.% metal content were prepared by 2-step incipient wetness impregnation. Between and after the impregnations, the catalysts were calcined in air at 373 K for 2 h and at 623 K for 5 h (heating rate of 1 K min^{-1}). The catalysts were labeled as xCuyCo/Al_2O_3, where x and y stand for copper and cobalt weight contents.

2.2. Catalyst characterization

The X-ray powder diffraction (XRD) experiments were performed using a Siemens D5000 diffractometer using Cu Kα radiation for crystalline phase detection. The average sizes of cobalt and copper oxide crystallites were calculated using the Co_3O_4 (3 1 1) diffraction peak at $2\theta = 36.96^\circ$ and CuO (1 1 1) diffraction peak at $2\theta = 35.5^\circ$, respectively, according to the Scherrer equation [44]. The *in situ* XRD patterns were measured during catalyst reduction in hydrogen (3% H_2 in Ar). The experiments were conducted by passing pure H_2 through the catalyst while increasing the temperature at a linear rate.

The *ex situ* X-ray absorption spectra at both Co and Cu absorption K edges (7709 and 8.979 eV, respectively) were measured at SNBL BM01B beam line, ESRF, France. The X-ray absorption measurements were performed in transmission mode; two ionization chambers were used for X-ray detection. The Si (1 1 1) channel cut monochromator was calibrated by setting the first inflection point of K-edge spectrum of Co and Cu foils. The X-ray absorption data were analyzed using the conventional procedure using ATHENA package [45]. The XANES spectra after background correction were normalized by the edge height. After subtracting the metal atomic absorption, the k^2-weighted EXAFS signal was transformed without phase correction from k space to r space. Crystalline Co_3O_4, CuO, and Cu_2O were used as reference compounds for XANES and EXAFS analysis.

The reducibility of the catalysts was studied by temperature-programmed reduction (TPR). The TPR was carried out by AutoChem II 2920 apparatus from Micromeritics using 0.05 g of the sample in 5 vol.% H_2/Ar stream (50 $cm^3\,min^{-1}$). The temperature was increased from room temperature to 1173 K at a rate of 3 K min^{-1}.

Surface analyses were performed using a VG ESCALAB 220XL X-ray photoelectron spectrometer (XPS) equipped with Al Kα (1486.6 eV) non-monochromatized source that was used for excitation with a 300 W-applied power. The analyzer was operated in a constant pass energy mode (E_{pass} = 40 eV). Binding energies were referenced to the Al_{2p} core level (74.6 eV) of the support. The vacuum level during experiments was better than 10^{-7} Pa. The powdered catalyst was pressed as a thin pellet onto a steel block. The reproducibility was 0.2 eV for the Co2p binding energy. The *in situ* reduction was carried out in pure hydrogen at 673 K in the reactor cell of the preparation chamber attached to the analysis chamber of the spectrometer. Then, the reduced sample was trans-

ferred to the analysis chamber of the XPS spectrometer; the preparation and analysis chambers were linked hermetically. The sample was transferred from the preparation to analysis chambers under vacuum without exposure to air.

Transmission electron microscopy (TEM) measurements were performed using a TECNA microscope operating at a voltage of 200 kV. The sample powder was ultrasonically dispersed in ethanol and deposited on a copper grid prior to the measurements.

The *in situ* magnetic measurements were performed using a Foner vibrating-sample magnetometer [46,47]. The magnetometer is fitted with a continuous flow quartz microreactor equipped with a built-in Pt–PtRh thermocouple. The experiments were conducted by passing pure H_2 through the catalyst while increasing the temperature from 293 to 873 K at a rate of 5 K min^{-1}; then, it was kept constant at 873 K. The sample amount for all measurements was around 20 mg. The appearance of ferromagnetic species in the samples was monitored *in situ* by a continuous increase in magnetization during the reduction. The temperature dependence of the saturation magnetization was measured at 280–873 K range with temperature ramp of 20 K min^{-1}. The magnetic properties of Cu–Co alloys have been a subject of numerous previous reports [48–51].

2.3. Catalytic reaction

Carbon monoxide hydrogenation reaction was carried out in a fixed bed stainless steel tubular microreactor ($d_{int.}$ = 13.1 mm). The average catalyst grain diameter was 100 μm. The influence of intraparticle diffusion limitations was evaluated using Weisz modulus [52]:

$$\Phi = \frac{r_a d^2}{D_{CO} C_{CO}}$$

where r_a is the reaction rate (mol/m^3 s), d is the catalyst grain diameter (m), D_{CO} is carbon monoxide diffusivity (m^2/s), and C_{CO} is carbon monoxide concentration (mol/m^3). The Weisz modulus was lower than 10^{-3} even with the most active Co/Al_2O_3 catalysts indicating the absence of intraparticle mass transfer limitations.

The thermocouple was put inside the reactor and was in direct contact with the catalyst, so the thermocouple measurement could reflect the temperature inside the reactor. No temperature spike and temperature swings were observed during steady state reactor operation.

The samples were reduced in hydrogen flow (50 cm^3/min) at 673 K for 5 h. Then, the reactor was cooled down to 453 K. After purging with Ar flow for 1 h, the premixed syngas with a molar ratio of H_2/CO = 2 was gradually introduced to the catalyst. Carbon monoxide contained 5% of nitrogen, which was used as an internal standard for calculating carbon monoxide conversion. The pressure was gradually raised to 20 bar. Then, the temperature was slowly increased to 523 K. A very slow ramp (<0.05 K/min) was used during the reactor startup with Co/Al_2O_3 catalysts to prevent possible reactor runaway [53]. The gaseous products were analyzed by on-line gas chromatography. Analysis of H_2, CO, CO_2, and CH_4 was performed using a packed CTR-1 column and a thermal conductivity detector. Gaseous hydrocarbons (C_1–C_7) were separated in a capillary Poraplot Q column and analyzed by a flame-ionization detector. The liquid products were collected in the trap kept at 283 K and analyzed offline by gas chromatography. The reaction was conducted for at least 48 h to avoid the inference of initial transient effects on the catalytic performance.

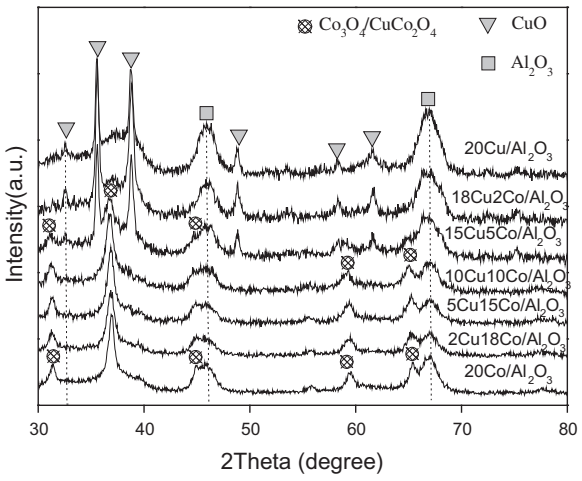

Fig. 1. XRD patterns of calcined monometallic and bimetallic Cu–Co catalysts.

3. Results

3.1. Calcined catalysts

The representative XRD patterns of calcined monometallic and bimetallic Cu–Co catalysts are displayed in Fig. 1. The XRD patterns of monometallic $20Co/Al_2O_3$ and $10Co/Al_2O_3$ catalysts were constituted by the peaks of characteristic of Co_3O_4 and γ-Al_2O_3. The monometallic $20Cu/Al_2O_3$ and $10Cu/Al_2O_3$ catalysts display the characteristic peaks of γ-Al_2O_3 and CuO. Table 1 shows that the cobalt oxide crystallite size estimated from the Scherrer equation [14] was about 13–14 nm in $20Co/Al_2O_3$ and $10Co/Al_2O_3$, while in the supported monometallic $10Cu/Al_2O_3$ and $20Cu/Al_2O_3$ catalysts, CuO forms relatively large crystallites (>25 nm). This observation and previous results for cobalt catalysts supported by Puralox-type alumina [37,54] suggest preferential localization of cobalt oxide particles in alumina pores (d_{pore} = 8 nm). Interestingly, an increase in cobalt content from 10 to 20 wt.% did not result in larger cobalt oxide crystallites (Table 1). The sizes of Co_3O_4 crystallites are slightly larger than the alumina pore diameter. This can be attributed [36] to a slightly elongated crystallite shape in mesopores, overestimation of crystallite size from the half-width of the diffraction profile [55], and discounting very small cobalt particles because of significant XRD line broadening. In monometallic $10Cu/Al_2O_3$ and $20Cu/Al_2O_3$ catalysts, copper oxide particles with the sizes larger than the alumina pore diameter seem to be located on the outer surface of alumina. Interestingly, the XRD patterns of calcined bimetallic catalysts with Cu/Co weight ratio <3 (molar ratio <2.78) exhibit only XRD patterns attributed to spinel structures such as Co_3O_4 or $CuCo_2O_4$ and γ-alumina. Note that because of similar cubic framework and almost identical unit cell parameters (a_{Co3O4} = 8.177 [56] and $a_{CuCo2O4}$ = 8.122 Å [57]) Co_3O_4 and $CuCo_2O_4$ are difficult to distinguish using their XRD patterns. The apparent spinel crystallite size estimated from the Scherrer equation decreases from 14 nm to 5 nm with an increase in copper contents (from 0 wt.% to 18 wt.%). Surprisingly, no XRD patterns assigned to monoclinic CuO were observed even at a relatively high copper content (10 wt.% Cu). The characteristic peaks of CuO began to appear when the copper content reached 15 wt.% (Cu/Co molar ratio increased to 2.78). This suggests that in bimetallic catalysts with relatively high copper content, no well-crystallized individual copper phase is present. XRD also did not show the presence of $CuCoO_2$ mixed oxide in the supported catalysts, which has been sometimes reported [11,58] in Cu–Co catalysts prepared by coprecipitation.

XPS and XAS have provided additional information about cobalt and copper phases and dispersions in the calcined catalysts. The XPS spectra of calcined cobalt and copper monometallic and bime-

Table 1
Crystallite sizes in the calcined alumina-supported Cu–Co catalysts.

Sample	Crystallite diameter by XRD		Cobalt concentration (wt.%)		Copper concentration (wt.%)	
	D ($M^{a}Co_2O_4$)/nm	D (CuO)/nm	XPS	Bulk	XPS	Bulk
$20Co/Al_2O_3$	14.1	–	–	–	–	–
$10Co/Al_2O_3$	13.5	–	2.0	10	0	0
$2Cu18Co/Al_2O_3$	10.5	–	–	18	–	2
$5Cu15Co/Al_2O_3$	10.9	–	3.7	15	2.6	5.0
$10Co10Cu/Al_2O_3$	9.6	–	3.2	10	5.1	10
$15Cu5Co/Al_2O_3$	6.4	26.0	2.4	5	16.2	15
$18Cu2Co/Al_2O_3$	5.0	25.3	–	2	–	18
$10Cu/Al_2O_3$	–	26.9	0	0	10.3	10.0
$20Cu/Al_2O_3$	–	25.6	–	–	–	–

[a] The average crystallite size of cobalt oxides ($MeCo_2O_4$ where Me = Co^{2+} or Cu^{2+}) was calculated according to the [3 1 1] diffraction peak at $2\theta = 36.7$. The average crystallite size of copper oxides was calculated according to the [1 1 1] diffraction peak at $2\theta = 35.5°$.

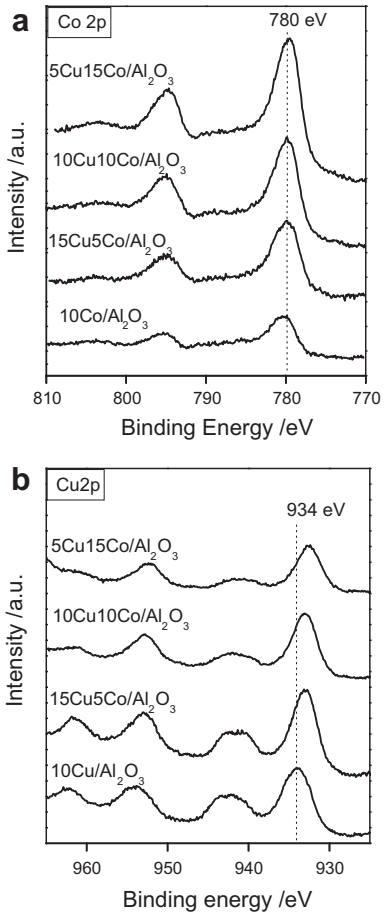

Fig. 2. Co2p (a) and Cu2p (b) XPS spectra of calcined Cu–Co catalysts.

tallic catalysts are shown in Fig. 2. The Co2p XPS spectra suggest the presence of Co_3O_4 in the subsurface layer of the calcined catalysts. This cobalt phase is generally identified by the binding energy at 780 eV, the spin–orbital splitting, and the absence of intense satellite structure [59,60]. Indeed, the $Co2p_{3/2}$ binding energy of our catalysts was 780 eV, and only very low intense satellites were observed. The Cu2p XPS spectrum of $10Cu/Al_2O_3$ suggests the presence of CuO detected by the peak at 934 eV assigned to CuO ($2p_{3/2}$), spin–orbital splitting, and satellites. The Cu $2p_{3/2}$ binding energies were lower for the supported bimetallic catalysts. The Cu/Co ratios measured by ICP in the bulk and by XPS in the subsurface layer are shown in Table 1 for the calcined catalysts. XPS indicates a much higher surface concentration of copper than cobalt in the calcined catalysts.

The energy-filtered TEM micrographs (Fig. 3) of $10Cu10Co/Al_2O_3$ catalyst indicate uniform chemical distribution of cobalt and copper. Cobalt oxide particles of 10–20 nm were detected by TEM. CuO particles were smaller than those of Co_3O_4. These particles form interfaces and interact with each other. The distance between the two adjacent planes, d, was measured to be 0.47 nm, which was characteristic of Co_3O_4. The d_{111} spacing of Co_2O_3 and CoO was 0.32 and 0.25 nm, far smaller than the d_{111} spacing of Co_3O_4 and $CuCo_2O_4$ (0.47 nm). Unfortunately, Co_3O_4 and mixed $CuCo_2O_4$ spinels cannot be clearly identified and distinguished from each other from interplanar spacings. This also confirms that Co_3O_4 and CuCo mixed spinels could be major cobalt phases in the calcined catalysts. The presence of smaller CuO particles was identified by d_{111} spacings of 0.23 nm [61,62].

Further information about cobalt and copper phases in the calcined catalysts was obtained by XANES/EXAFS. The XANES, derivative XANES spectra, and EXAFS Fourier transform moduli of calcined Cu–Co catalysts and reference compounds measured at Cu and Co K-absorption edges are shown in Figs. 4, 5 and 6. Co_3O_4 is a spinel structure with two types of cobalt sites (Co^{2+} and Co^{3+}). In Co_3O_4, Co^{2+} and Co^{3+} ions have respectively tetrahedral and octahedral coordinations. Therefore, the XANES spectrum of Co_3O_4 is a superposition of the spectra of Co^{2+} and Co^{3+} ions. XANES spectra identical to that of Co_3O_4 were previously observed for monometallic Co/Al_2O_3 catalysts [63,64]. Fig. 4 shows that the Co XANES spectra evolve with an increase in copper content. This corresponds to the decrease in the intensity of the lower energy contribution of XANES spectrum that could be due to the absorption edge of Co^{2+} sites. Hence, the presence of copper in mixed Cu–Co catalysts could result in decrease in the concentration of Co^{2+} ions.

Table 2 displays data about coordination of Co^{2+} and Co^{3+} ions in Co_3O_4 spinel. The influence of local coordination of cobalt in spinel structure of Fourier transform modulus was investigated using FEFF code [65]. Four peaks at 1.50, 2.48, 3.00, and 4.70 Å are observed in the moduli of Fourier transform of cobalt EXAFS (Fig. 6a). In accordance with previous reports [38,66,67], the first peak at 1.50 Å is attributed to first CoO coordination shells for octahedral Co^{3+} ($d = 1.912$ Å) and tetrahedral Co^{2+} sites ($d = 1.943$ Å). These two CoO coordination shells are usually not resolved in the Fourier transform moduli [38,66,67]. On the basis of FEFF simulations, the peaks situated at 2.48 and 3.00 Å, respectively, were assigned to Co^{3+}–Co^{3+} ($d = 2.854$ Å) and to both Co^{3+}–Co^{2+} ($d = 3.346$ Å) and Co^{2+}–Co^{2+} ($d = 3.495$ Å) coordination shells in Co_3O_4 (Table 2). The peak at 4.70 Å was attributed to the Co^{2+}–Co^{3+} distance of 5.244 Å. The $CuCo/Al_2O_3$ catalysts with different Cu or Co contents showed cobalt EXAFS Fourier transform moduli similar to Co_3O_4 (Fig. 6a). Thus, cobalt ions in the alumina-supported Cu–Co catalysts have local coordination close to that in spinel with possibly some enrichment in Co^{3+} ions at higher copper

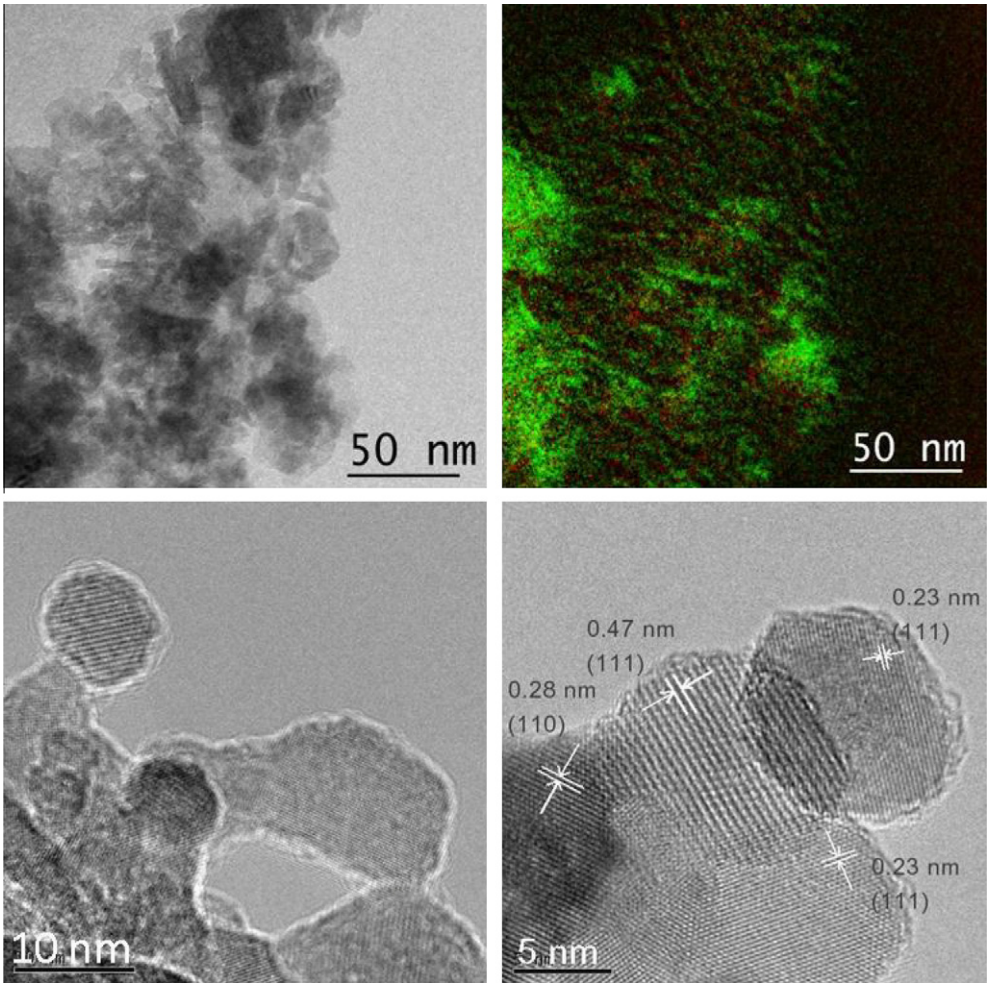

Fig. 3. EFTEM and TEM images of calcined 10Cu10Co/Al_2O_3 catalyst (Co green, Cu red). (For interpretation of the references to color in this figure legend, the reader is referred to the web version of this article.)

contents. Interestingly, FEFF modeling showed only slight influence of substitution of Co^{2+} by Cu^{2+} ions in spinel structure on the EXAFS Fourier transform modulus.

The XANES and derivative XANES spectra of the Cu–Co catalysts at Cu absorption edge were compared with XANES spectra of CuO and Cu_2O reference compounds (Fig. 5). The XANES results of the calcined catalysts at Cu absorption edge are within the range expected for Cu^{2+} ions. The XANES spectrum of CuO has two distinguishable features characteristic of Cu^{2+} ($3d^9$) compounds [68] with a small pre-edge absorption at 8978 eV and a shoulder at 8986 eV, which is assigned to the 1s–4p "shake down" transition. However, relative to crystalline CuO, the calcined catalysts have a more intense white line (first peak after the absorption edge), indicating a higher 4pσ density of states [69]. The Fourier transform moduli of EXAFS for the catalysts with higher copper contents resemble the references data for crystalline CuO (Fig. 6b). Broader and lower intense radial distribution peaks for the second and third CuCu coordination shells at 2.54, 3.01, and 5.61 Å in the calcined catalysts indicate smaller sizes of CuO particles and higher Debye–Waller factor. Note that the Fourier transform modulus of the 5Cu15Co/Al_2O_3 catalyst with smaller copper content is rather different from the EXAFS Fourier transform modulus of CuO and Cu–Co catalysts containing higher amounts of copper. It looks similar to the Fourier transform modulus of Co_3O_4. The peak in EXAFS Fourier transform modulus in 5Cu15Co/Al_2O_3 at 4.90 Å, which is almost absent in the samples with high copper content, seems to be attributed to Cu^{2+}–Co^{3+} distances in mixed $Cu_xCo_{3-x}O_4$ phase. Modeling EXAFS data using FEFF code suggests that 5Cu15Co/Al_2O_3 catalyst contains both CuO and mixed Cu–Co oxide phases. In the mixed Cu–Co oxide phase, a significant fraction of Cu^{2+} ions have local coordination similar to that of Co^{2+} ions in Co_3O_4. This is confirmed by a peak in EXAFS Fourier transform modulus at 4.90 Å. This type of copper coordination was previously observed in $Cu_xCo_{3-x}O_4$ spinels [57,70]. Thus, a noticeable concentration of $Cu_xCo_{3-x}O_4$ mixed compounds seems to be present in the calcined bimetallic Cu–Co catalysts.

3.2. Catalyst reduction

The H_2-TPR profiles of 20Co/Al_2O_3 monometallic cobalt catalyst supported on Al_2O_3 (Fig. 7) display two hydrogen consumption peaks. In agreement with previous reports [38,66,71,72], these peaks correspond to two steps reduction of Co_3O_4 into metallic cobalt, which proceeds via intermediate formation of CoO. Reduction of smaller CoO particles into metallic cobalt proceeds particularly difficult and requires higher temperatures. It corresponds to the high-temperature broad TPR peak. The monometallic copper catalyst shows a single reduction peak at 493 K, which probably corresponds to the single step reduction of CuO into metallic copper. For bimetallic samples, the H_2-TPR profiles are more complex; they show several reduction steps. These peaks could be assigned to the reduction of Co_3O_4 and CuO to partially reduced oxide

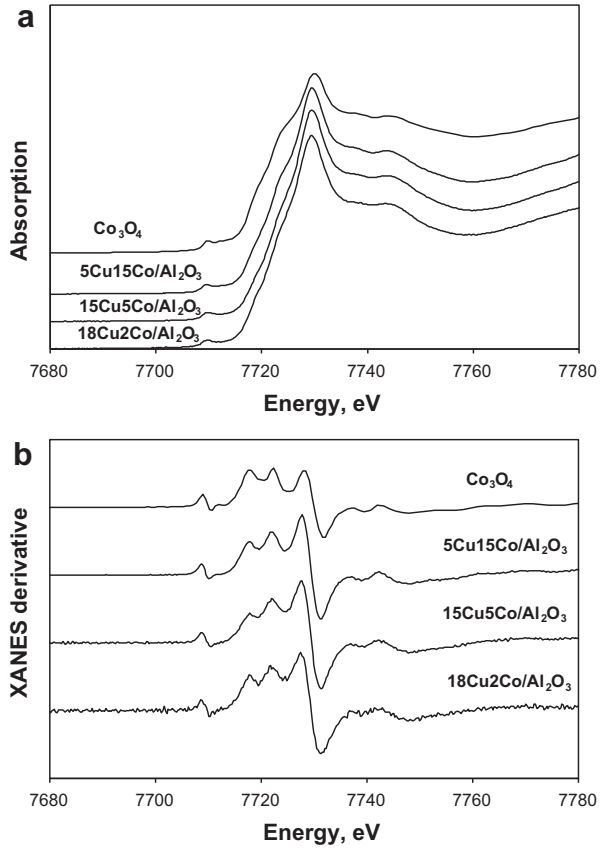

Fig. 4. XANES (a) and XANES derivative (b) at Co K-absorption edge of calcined Cu–Co catalysts.

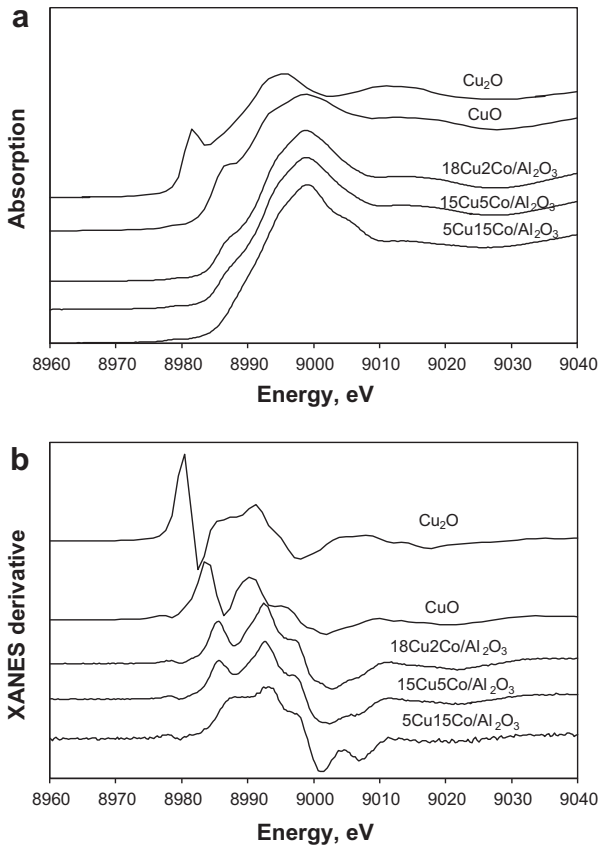

Fig. 5. XANES (a) and XANES (b) derivative at Cu K-absorption edge of calcined Cu–Co catalysts.

species and ultimately to copper and cobalt metal phases. XANES/EXAFS showed a strong interaction between cobalt and copper in the calcined catalysts, which could lead to the formation of non-stoichiometric spinel $Co_{1-x}Cu_xCo_2O_4$ [57,70]. Therefore, it is reasonable to suppose that some peaks in the H_2-TPR profiles of the bimetallic catalysts can be attributed to the reduction of these mixed CuCo oxides. Note that addition of even smaller amounts of copper results in dramatic decrease in temperature of catalyst reduction. The enhanced reducibility of the precipitated cobalt catalysts in the presence of copper was previously reported by Baillard-Letoumel et al. [73]. The formation of easy reducible mixed CuCo species and possible hydrogen activation on the reduced copper sites could probably explain the shift of reduction peaks to lower temperatures with increasing copper contents.

The *in situ* XRD measurements were used to provide further insights into the genesis of active phases in monometallic and bimetallic Cu–Co catalysts. The samples were reduced by passing 3%H_2/Ar through the catalyst while increasing the temperature with simultaneous XRD analysis. The *in situ* XRD patterns of 20Co/Al_2O_3 catalyst (Fig. 8a) show reduction of Co_3O_4 phase into CoO which starts at 573 K. CoO then can be reduced completely to Co^0 when the temperature reaches 1073 K. In agreement with previous reports [41,42,74], metallic cobalt is present as mostly cobalt fcc cubic phase. These observations are consistent with TPR and magnetization measurements.

In the bimetallic 10Cu10Co/Al_2O_3 catalyst, the reduction of Co_3O_4 phase to CoO appears to proceed at a lower temperature (~473 K) (Fig. 8b). The *in situ* XRD patterns of the catalysts reduced at 523 K show the peaks located at $2\theta = 43.8°$ and 50.9°, while in cobalt fcc phase, these peaks are located at $2\theta[111] = 45.9°$ and $2\theta[200] = 53.5°$ [75]. This is consistent with a previous report by Volkova et al. [58], who also observed appearance of Co–Cu mixed metallic phases on reduction of Cu–Co mixed oxide with interspacing parameters that were intermediate between copper and cobalt fcc metallic phases. This suggests the formation of Cu–Co alloys in the reduced bimetallic catalysts.

The magnetic method, which is selectively sensitive to the presence of ferromagnetic phases, has provided additional information about catalyst reducibility and structure of reduced cobalt and copper metallic phases. Fig. 9 shows the magnetization curves of 10Co/Al_2O_3, 20Co/Al_2O_3, and bimetallic Co–Cu/Al_2O_3 catalysts during temperature ramping in hydrogen. No noticeable variation of magnetization was observed during the reduction of copper monometallic catalyst, because copper does not form any ferromagnetic phases. The magnetization measurements for monometallic cobalt catalysts show appearance of cobalt–metal ferromagnetic phase at 600 K. Promotion of this catalyst with copper results in a remarkable decrease in the temperature of the emergence of ferromagnetic phases. This observation is consistent with TPR measurements (Fig. 7), which also indicate much easier catalyst reducibility in the presence of small amounts of copper. The value of magnetization obtained in the catalysts after reduction increases with higher cobalt contents in the catalysts. Quantitative analysis of magnetization values suggests that higher extent of cobalt reduction (>80%) in the supported Cu–Co catalysts could be achieved at much lower temperatures than in cobalt monometallic counterparts.

The measured field dependence curves with hysteresis loop [46,47] (not shown) indicate the presence of ferromagnetic particles in the reduced catalysts. To identify the formation of mixed Co–Cu metallic phases, the dependence of magnetization at saturation in the reduced samples was measured as a function of temper-

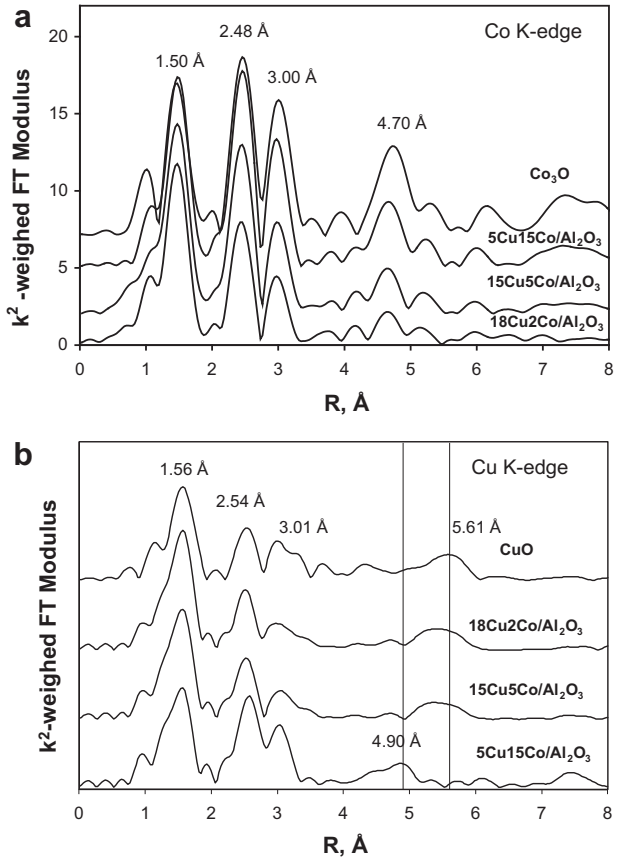

Fig. 6. EXAFS Fourier transform moduli at Co (a) and Cu K (b)-absorption edges of calcined Cu–Co catalysts.

Table 2
Cobalt coordination in crystalline Co_3O_4 ($Co^{2+}Co^{3+}{}_2O_4$).[a]

Central ion	Neighbor	Coordination number	Distance (Å)
Co^{2+}	O	4	1.943
	Co^{3+}	12	3.346
	O	12	3.386
	Co^{2+}	4	3.495
	O	12	4.271
	O	12	5.092
	Co^{3+}	16	5.244
	O	4	5.439
	Co^{2+}	12	5.708
Co^{3+}	O	6	1.912
	Co^{3+}	6	2.854
	O	2	3.300
	Co^{2+}	6	3.346
	O	6	3.565
	O	24	4.466
	O	12	4.666
	Co^{3+}	12	4.943
	Co^{2+}	8	5.244
	Co^{3+}	12	5.708
	O	6	5.866

[a] Interatomic distances smaller than 6 Å.

ature. Fig. 10 displays thermomagnetic curves obtained for monometallic cobalt catalyst and CoCu counterparts with different copper contents. As expected, the magnetization drops with temperature that corresponds to thermal disordering of ferromagnetic domains. Note, however, that the decrease in magnetization with temperature is more pronounced when copper is present in the catalysts. This seems to be an indication of formation of bimetallic

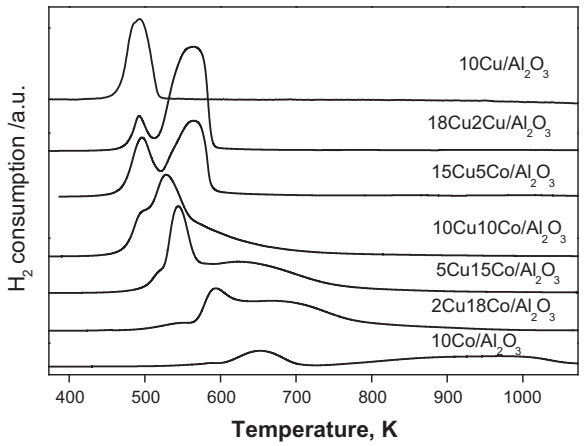

Fig. 7. H_2-TPR profiles of Cu–Co catalysts.

Cu–Co particles that have different ferromagnetic properties relative to metallic cobalt. Indeed, if only individual monometallic cobalt or copper particles were present, the thermomagnetic curve should be identical to that observed with the monometallic Co/Al_2O_3 catalyst.

XPS was used for identification of different cobalt species in the catalysts reduced *in situ* in H_2 at 673 K (Fig. 11). Cobalt and copper metal phases were identified in the XPS spectra by binding energies ($Co2p_{3/2}$ = 778 eV [76], $Cu2p_{3/2}$ = 932.6 eV [77]), spin–orbital splitting, and line shape. The results suggest almost complete reduction of copper to the metallic state (Fig. 11a), while both cobalt metallic species and CoO were detected (Fig. 11b). The extent of cobalt reduction was higher in bimetallic $10Cu10Co/Al_2O_3$ (>50%) than in monometallic $10Co/Al_2O_3$ (~30%). Copper surface concentration was much higher than concentration of cobalt in both calcined and reduced catalysts (Table 3).

3.3. Catalytic performance

The catalytic data are shown in Tables 4 and 5. The catalytic performance was evaluated after 48 h of the reaction after stabilization of catalytic activity. No visible deactivation was observed after 48 h on-stream. Hydrocarbons, alcohols, and water were the major reaction products; low selectivity to CO_2 was observed under our reaction conditions. In agreement with previous results [37,54,64], the monometallic cobalt catalyst exhibited higher activity in Fischer–Tropsch synthesis producing mostly medium-chain and long-chain hydrocarbons with only trace concentrations of alcohols. The carbon monoxide hydrogenation activity of monometallic copper catalyst was much lower under the same reaction conditions; methanol and water were major reaction products with smaller concentrations of hydrocarbons. Addition of even small amounts of copper to Co/Al_2O_3 leads to a 10 times higher selectivity for alcohol synthesis and immediate drop in overall activity. Promotion of cobalt catalysts with copper also affects hydrocarbon selectivity. While $10Co/Al_2O_3$ catalyst under the reaction conditions showed 30% selectivity to C_{7+} hydrocarbons, no long-chain hydrocarbons were detected in the bimetallic Cu–Co catalysts even with low copper loadings (Table 5). A monometallic copper catalyst makes methanol with selectivity more than 85%, while the bimetallic catalysts are more selective to lighter hydrocarbons and higher alcohols.

4. Discussion

The characterization and catalytic studies show that the structure and catalytic performance of bimetallic Cu–Co catalysts

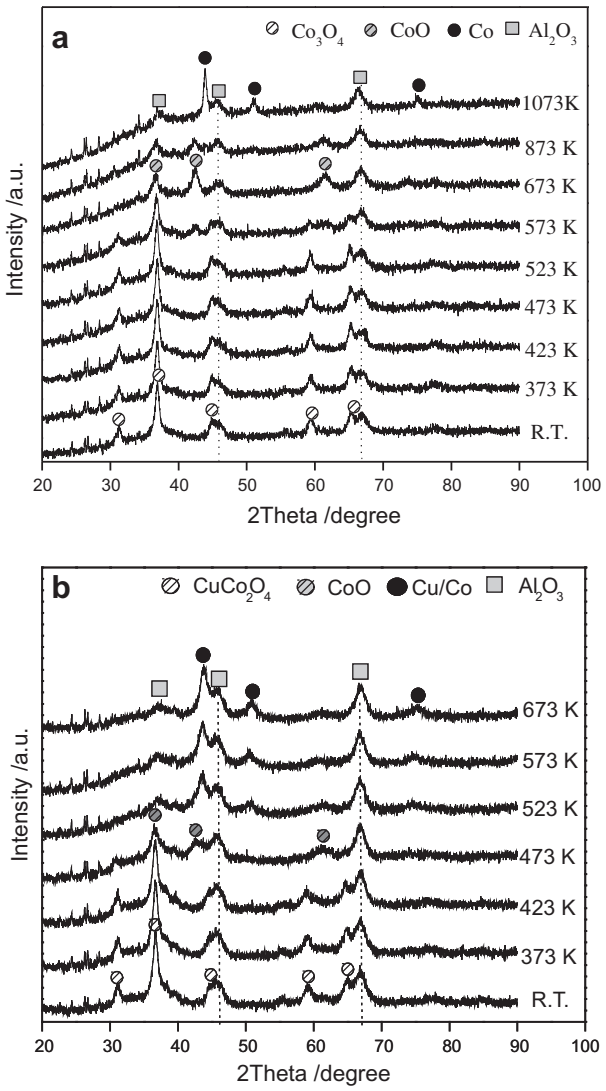

Fig. 8. *In situ* XRD patterns of $20Co/Al_2O_3$ (a) and $10Cu10Co/Al_2O_3$ (b) taken during reduction of Cu–Co catalysts in 3% H_2/Ar.

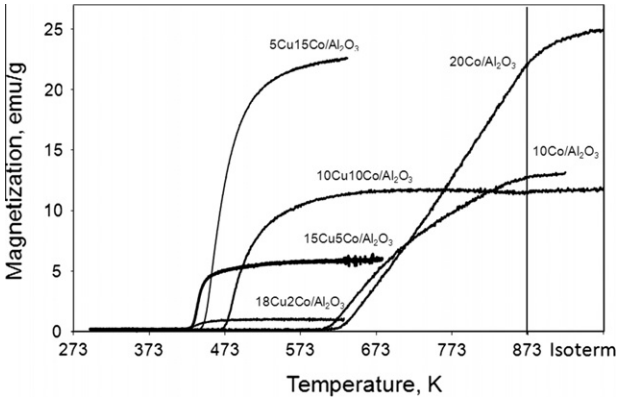

Fig. 9. Catalyst magnetization during reduction in pure hydrogen (ramp 5 K min^{-1}).

prepared via impregnation are much different from the monometallic counterparts. Calcined monometallic cobalt and copper catalysts contain Co_3O_4 and CuO crystallites respectively, while the presence of mixed $CuCo_2O_4$ oxide has been detected in bimetallic catalysts. In the catalysts with lower copper content, Cu^{2+} ions

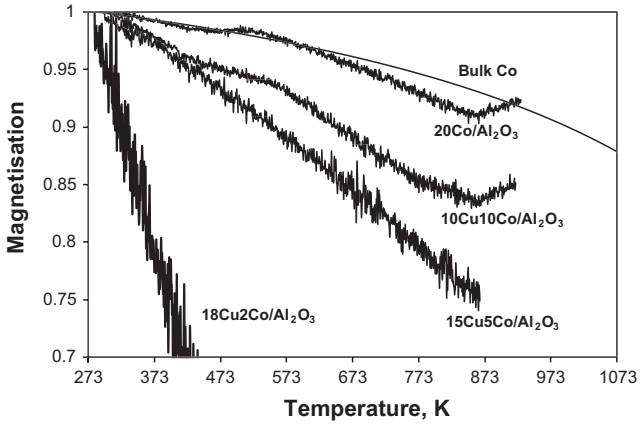

Fig. 10. Thermomagnetic curves of reduced Cu–Co catalysts. Magnetization is measured at saturation. Temperature ramp 20 K min^{-1}. The catalysts were reduced in H_2 at 673 K.

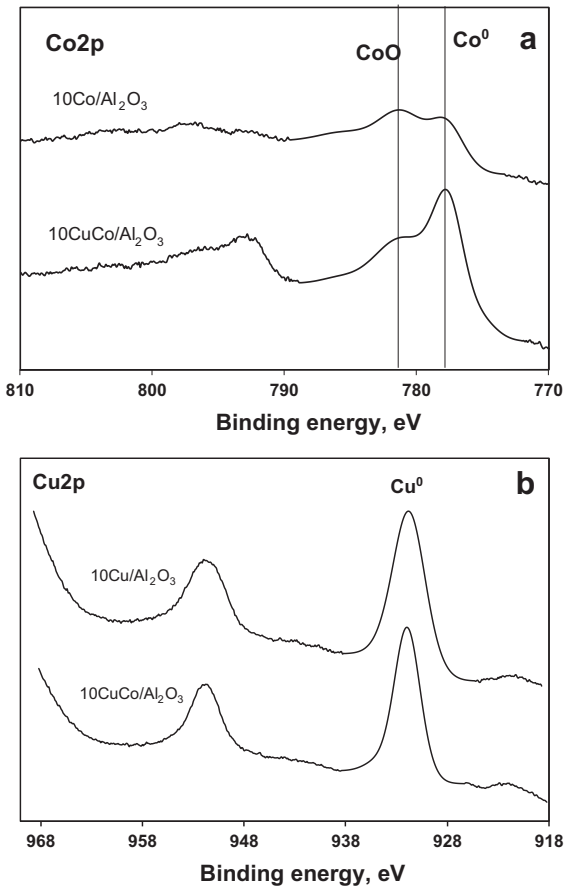

Fig. 11. Co2p and Cu2p XPS spectra of the catalysts reduced *in situ* in H_2 at 673 K.

seem to be partially incorporated in the structure of Co_3O_4 type spinel. This is consistent with the absence of CuO diffraction patterns for copper–cobalt bimetallic catalysts, lower contribution of Co^{2+} ions to Co K-absorption edge (Fig. 4a and b), and local copper coordination in the catalysts with lower copper content similar to that of Co^{2+} ions in Co_3O_4.

The presence of even small amounts of copper results in a significant enhancement of catalyst reducibility. This is probably due to the fact that copper and mixed Cu–Co species can be reduced to metallic state at lower temperature than cobalt oxides.

Table 3
Bulk and surface copper and cobalt concentration in the reduced catalysts.

Sample	Cobalt concentration (wt.%)			Copper concentration (wt.%)		
	Bulk (ICP)	Surface (XPS)	Surface/bulk	Bulk (ICP)	Surface (XPS)	Surface/bulk
$10Co/Al_2O_3$	10	1.0	0.1	0		
$10Cu10Co/Al_2O_3$	10	2.0	0.2	10	4.0	0.4
$10Cu/Al_2O_3$	0	–		10	4.0	0.4

Table 4
Catalytic performances of Cu–Co catalysts in carbon monoxide hydrogenation.

Catalyst[a]	CO conv. (%)	GHSV ($ml/g_{cat}/h$)	Time yield ($mmol/h\ g_{cat}$)[b]	Carbon selectivity (C mol%)[c]			Total alc. STY ($mg/g_{cat}\ h$)[d]
				HC	ROH	CO_2	
$10Co/\gamma\text{-}Al_2O_3$	36.6	28,800	149.1	97.7	1.9	0.4	Trace
$5Cu15Co/Al_2O_3$	30.9	4500	19.6	88.5	10.3	1.2	43.8
$10Cu10Co/Al_2O_3$	16.5	3600	8.5	82.6	17.1	0.3	20.6
$15Cu5Co/Al_2O_3$	23.2	1800	6.0	75.6	23.3	1.1	25.0
$18Cu2Co/Al_2O_3$	12.7	1800	3.2	77.7	20.9	1.3	9.5
$20Cu/\gamma\text{-}Al_2O_3$	25.2	900	3.2	10.9	85.8	3.3	39

[a] Catalyst (Ratio of Co/Cu) 2.0 g mixed with 3.0 g SiC(0.062 mm), *in situ* reduction in H_2 at 673 K for 5 h before reaction.
[b] Reaction conditions: Temp. = 523 K; P = 20 bars; R (H_2/CO) = 2, Time yield ($mmol/(g_{cat}\ h)$ = conv.% * F_{CO} (mol/h)/$w_{cat}(g)$ * 1000.
[c] Carbon selectivity is defined as the selectivity of all the carbon-containing products formed from converted carbon, and the values are recalculated from the original data; HC = total hydrocarbons including methane; ROH = total alcohol including methanol.
[d] Total alc. STY = space time yield of alcohols.

Table 5
Products distributions for hydrocarbon and alcohol product family. The reaction conditions, conversions, and GHSV are from Table 4.

Catalyst	Hydrocarbons distribution (C mol%)				Alcohol distribution (wt.%)[a]		
	CH_4	$C_{2-4}H$	$C_{5-7}H$	$C_{7+}H$	MeOH	EtOH	$C_{3+}OH$
$10Co/Al_2O_3$	31.1	30.8	5.4	30.4	2.6	1.4	95
$5Cu15Co/Al_2O_3$	51.0	31.5	5.9	0	43.1	37.1	19.8
$10Cu10Co/\gamma\text{-}Al_2O_3$	37.1	33.9	11.7	0	35.7	43.7	20.5
$5Co15Cu/Al_2O_3$	32.8	32.2	10.6	0	20.7	34.7	44.5
$2Co18Cu/Al_2O_3$ (1:9)	30.3	34.1	13.3	0	58.5	17.4	24.1
$20Cu/Al_2O_3$	10.9	No	No	0	99.5	0.2	0.3

[a] Alcohol distribution (wt.%): the proportion of each alcohol in the total value; $C_{3+}OH$ = alcohol of C number higher than 2.

Previous reports [78–80] indicate dissociative hydrogen adsorption on metallic copper with very low activation barrier [70]. Similar effects have been observed after promotion of cobalt catalysts with noble metals [7]. Thus, reduced metallic Cu and Cu–Co particles could activate hydrogen for the reduction of more hardly reducible cobalt species. The reduction of the catalysts leads to the increase in magnetization measured *in situ* using Foner magnetometer. Formation of Cu–Co bimetallic particles was observed at relatively lower temperatures (423–473 K). These particles could further catalyze the reduction of cobalt species. This observation is consistent with previous *ex situ* magnetic results for cobalt–copper coprecipitated catalysts [81]. In contrast to the results of Courty and Chaumette [82] for the coprecipitated catalysts, the extent of cobalt reduction was rather high in the supported Cu–Co counterparts. Note that higher concentration of cobalt containing ferromagnetic metallic phase was detected at relatively lower temperature. Thus, the *in situ* magnetic measurements could attribute the activity of copper–cobalt catalysts in carbon monoxide hydrogenation to bimetallic Cu–Co particles [18,28,29].

The formation of Cu–Co bimetallic particles has also been confirmed by thermomagnetic curves. The thermomagnetic curve measured for monometallic supported cobalt catalyst is almost identical to that to bulk cobalt. The presence of copper in the catalysts modifies the thermomagnetic curves. In the presence of copper, the magnetization drops much more rapidly with temperature. Note that the decrease of magnetization with temperature suggests significant interaction between copper and cobalt. The modification of ferromagnetic properties should occur if cobalt and copper mixed together in the metal particles forming alloys. The modification of ferromagnetic properties is not expected in cobalt core–copper shell particles. In the core–shell particles, the cobalt and copper phases are nearly separated and the concentration of Cu–Co alloy should be smaller.

The catalytic results are consistent with the characterization data. The catalytic performance of Cu–Co alloys seems to be rather different from monometallic copper or cobalt species. The addition of even small amounts of copper during impregnation results in significant modification of catalytic performance. The selectivity seems to be modified to a greater extent, while the carbon monoxide hydrogenation rates decrease 7–8 times. Medium-chain and long-chain hydrocarbons are the principal products of carbon monoxide hydrogenation on the cobalt catalyst. The cobalt turnover frequency (TOF, reaction rates normalized by the total number of Co atoms on the surface of metal particles) for $10Co/Al_2O_3$ catalyst was calculated from reaction rates, extent of cobalt reduction and cobalt dispersion. Co dispersion was calculated from XRD Co_3O_4 particle size (Table 1) using the formulas from Ref. [83]: $D_{Co} = 96/d_{Co}$ (nm), $d_{Co} = 0.75d_{Co3O4}$. The extent of cobalt reduction (~30%) was estimated from XPS data for the reduced catalysts. The calculation yields TOF $\approx 0.8\ s^{-1}$ for $10Co/Al_2O_3$ at 523 K, $H_2/CO = 2$ and P = 20 bar. This value is somewhat higher than cobalt TOF measured under typical conditions of Fischer–Tropsch synthesis (T = 473–493 K) [84–86], which is probably due to higher reaction temperature in our carbon monoxide hydrogenation experiments

than during the Fischer–Tropsch reaction (T = 523 K versus 473–493 K).

Methanol was the major product with 85% selectivity over the monometallic $20Cu/Al_2O_3$ catalyst. The monometallic copper catalysts contain only copper active metal sites. The number of active sites for methanol synthesis was calculated from XRD patterns of oxidized catalyst assuming copper particle shrinking after reduction according to the molar volumes of CuO and metallic Cu: $d_{Cu} = 0.86 d_{CuO}$. Copper dispersion was calculated from copper metal particle size using the formula: $D_{Cu},\% = 104/d_{Cu}$ (nm) [87]. XPS data indicate complete copper reduction after treatment with hydrogen at 673 K (Fig. 11). The copper turnover frequency (defined similarly to cobalt TOF) was calculated using the carbon monoxide hydrogenation rate (Table 4) and copper dispersion. The TOF at 523 K, $H_2/CO = 2$, and P = 20 bar was 5.97×10^{-3} s^{-1} for $20Cu/Al_2O_3$ catalyst that is consistent with previous reports about the activity of copper methanol synthesis catalysts [88–90]. This suggests much lower intrinsic activity of copper metal sites in carbon monoxide hydrogenation than that of cobalt sites.

The bimetallic Cu–Co catalysts show that the selectivity is very different to those observed on monometallic cobalt and copper catalysts. No production of long-chain (C7+) hydrocarbons has been observed over the bimetallic catalysts, and the bimetallic catalysts exhibit higher selectivity to C2+ alcohols and higher selectivity to lighter hydrocarbons. Note that major changes in the reaction rates and selectivities occur at relatively low copper content. The *in situ* magnetic measurements indicate high cobalt extent of reduction. Characterization data showed some enhancement of metal dispersion (Table 1) in the catalysts while the catalyst reducibility seems to be significantly improved in the presence of even small amounts of copper. The thermomagnetic curves indicate formation of Cu–Co alloy particles, while XPS (Table 3) suggests some increase in copper concentration in the reduced catalysts. These observations suggest that carbon monoxide hydrogenation over Cu–Co catalysts prepared by co-impregnation proceeds on Cu–Co bimetallic particles that could be enriched with copper atoms on the outer surface. The formation of Cu–Co bimetallic particles enriched on outer surface with copper is consistent with the thermodynamic data. Indeed, it is known [91] that Cu and Co show limited miscibility in the Cu–Co alloys. The surface energy of copper (1.934 J M^{-2}) is smaller than that of cobalt (2.709 J M^{-2}) [92], which could result in preferential localization of copper on the particle surface. The concept of active sites for carbon monoxide hydrogenation in supported Cu–Co catalysts, which would involve copper and partially reduced cobalt species, seems to be less credible. Indeed, if the active sites involve ionic cobalt, it would difficult to explain the dramatic drop of catalytic activity after the addition of small amounts of copper to the cobalt monometallic catalyst (Table 4). Characterization results suggest that on copper addition to cobalt catalysts, both cobalt reducibility and cobalt dispersion have been enhanced.

Thus, the bimetallic catalysts seem to contain several types of active sites that could be associated to copper, copper–cobalt alloy, and cobalt nanoparticles. The TOF of cobalt sites in carbon monoxide hydrogenation is two orders of magnitude higher than of copper sites. A significant decrease in carbon monoxide reaction rates on addition of small amount of copper to cobalt catalysts suggests preferential localization of cobalt inside the metal particles where cobalt atoms are not available for the reaction. An attempt was made to evaluate the TOF in carbon monoxide hydrogenation on bimetallic catalysts, assuming formation of Cu–Co bimetallic particles with extent of cobalt reduction of about 60% and metal dispersion calculated from XRD data (Table 1). The estimated TOF (about $\sim 10^{-2}$ s^{-1}) confirms a significant drop of per site activity in the bimetallic catalysts after addition of copper. Previous reports suggest [86,93,94] that for the supported cobalt catalyst, the carbon monoxide hydrogenation rate for cobalt nanoparticles larger than 6–8 nm is proportional to the number of cobalt surface atoms. The catalytic activity of alloy particles is not only a function of particles sizes but also dependent on the surface and bulk compositions of the bimetallic particles. It appears that the turnover frequency in carbon monoxide hydrogenation on mixed copper cobalt particles remarkably drops with higher fraction of copper.

Our present results suggest that the selectivity to higher alcohols on supported copper–cobalt bimetallic particles remains, however, rather limited. Chemical promotion combined with optimization of metal particle size and fraction of copper and cobalt in the bimetallic clusters might be efficient routes to further enhance alcohol selectivity over supported Cu–Co catalysts.

5. Conclusions

A combination of various characterization techniques allowed a clear picture of the genesis of active sites in supported copper–cobalt catalysts to be developed. XRD and XAS indicated a higher dispersion of copper than cobalt in the calcined supported catalysts. A strong interaction between cobalt and copper oxide particles, which leads to $CuCo_2O_4$ mixed spinel, was further confirmed by EXAFS. TPR and *in situ* magnetic measurements showed a much easier reduction of cobalt in the presence of copper. The *in situ* magnetic measurements also showed a formation of bimetallic Cu–Co particles in the reduced catalysts. The catalytic studies have shown a dramatic modification of carbon monoxide hydrogenation rate and selectivity after addition of even smaller amounts of copper to supported cobalt catalysts. The selectivity to alcohols increases several times, while overall carbon monoxide conversion decreased. Both the characterization and catalytic studies suggest formation of bimetallic Cu–Co species and enrichment of the surface of the bimetallic particles with copper. These bimetallic copper–cobalt particles could be involved in alcohol synthesis over the supported Cu–Co catalysts.

Acknowledgments

J.W. thanks the PhD scholarship support of the China Scholarship Council. The authors thank J. Deleplanque, A. Beaurain, L. Burylo, O. Gardoll, O.V. Safonova, and Jing Fangli for help with alcohols analysis, XPS, X-ray diffraction, TPR, XAS, and catalytic reactor, respectively. C. Pham-Huu and O. Ersen from University of Strasbourg are acknowledged for their expertise in TEM measurements. M. Olea from the Teesside University is acknowledged for help with copper reference compounds. The authors would like to thank the colleagues in the Unité de catalyse et de chimie du solide, UMR CNRS 8181 of France and those of Lab of Xiamen University for useful discussions. The Swiss-Norwegian Beamlines and ESRF are acknowledged for use of synchrotron radiation. Y.W. acknowledges the financial support from the National Natural Science Foundation of China (Nos. 20923004 and 21033006). P.A.C. acknowledges the financial support of the Russian Foundation for Fundamental Research (Grants # 03-00501-a and # 11-02-90493-Ukr_f_a).

References

[1] P. Forzatti, E. Tronconi, I. Pasquon, Catal. Rev. Sci. Eng. 33 (1991) 109.
[2] J.J. Spivey, A. Egbebi, Chem. Soc. Rev. 36 (2007) 1514.
[3] V. Subramani, S.K. Gangwal, Energy Fuel 22 (2008) 814.
[4] N. Tsubaki, S. Sun, K. Fujimoto, J. Catal. 199 (2001) 236.
[5] F. Morales, B.M. Weckhuysen, Catal. Roy. Soc. Chem. 19 (2006) 1.
[6] R. Oukaci, A.H. Singleton, J.G. Goodwin, Appl. Catal. A 186 (1999) 129.
[7] F. Diehl, A.Y. Khodakov, Oil Gas Sci. Technol. 64 (2009) 11.
[8] G.L. Bezemer, P.B. Radstake, U. Falke, H. Oosterbeek, H.P.C.E. Kuipers, A.J. van Dillen, K.P. de Jong, J. Catal. 237 (2006) 152.

[9] J.P. den Breejen, A.M. Frey, J. Yang, A. Holmen, M.M. van Schooneveld, F.M.F. de Groot, O. Stephan, J.H. Bitter, K.P. de Jong, Top. Catal. 54 (2011) 768.
[10] Report on Investigations by Fuels and Lubricants Teams at the I.G. Farbenindustrie A.G. Works at Leuna. In: R. Holroyd (Ed.), 24th September 1945. <http://www.fischer-tropsch.org/primary_documents/gvt_reports/MofFP/ig_farb_at_leuna/ig_toc.htm>.
[11] G.T. Krieger, L. Plyasova, V. Zaikovskii, T. Yurieva, Stud. Surf. Sci. Catal. 107 (1997) 67.
[12] G.G. Volkova, PhD Thesis, Boreskov Institute of Catalysis, Novosibirsk, Russia, 1997.
[13] A. Kiennemann, R. Breault, J.-P. Hindermann, M. Laurin, J. Chem. Soc. Faraday Trans. 1 (83) (1983) 2119.
[14] V.R. Surisetty, A.K. Dalai, J. Kozinski, Energy Fuels 24 (2010) 4130.
[15] V.R. Surisetty, A.K. Dalai, J. Kozinski, Ind. Eng. Chem. Res. 49 (2010) 6956.
[16] H. Arakawa, T. Fukushima, M. Ichikawa, S. Natsushita, K. Takeuchi, T. Matsuzaki, Y. Sugi, Chem. Lett. (1985) 881.
[17] S. Ishiguro, S. Ito, K. Kunimori, Catal. Today 45 (1998) 197.
[18] P. Courty, D. Durand, E. Freund, A. Sugier, J. Mol. Catal. 17 (1982) 241.
[19] A. Razzaghi, J.P. Hindermann, A. Kiennemann, Appl. Catal. 13 (1984) 193.
[20] A. Kiennemann, C. Diagne, J.P. Hindermann, P. Chaumette, P. Courty, Appl. Catal. 53 (1989) 197.
[21] P. Courty, D. Durand, A. Sugier, E. Freund, UK Patent 2118061A, 1983.
[22] P. Courty, D. Durand, A. Sugier, E. Freund, UK Patent 2158730, 1983.
[23] P. Chaumette, P. Courty, D. Durand, P. Grandvallet, C. Travers, US Patent 4791141, 1988.
[24] P. Courty, H. Ajot, Ch. Marcilly, Powder Technol. 7 (1973) 21.
[25] G.R. Sheffer, T.S. King, Appl. Catal. 44 (1988) 153.
[26] X. Xu, B.M. Doesburg, I.I.F. Scholten, Catal. Today 2 (1987) 125.
[27] V. Mahdavi, M.H. Peyrovi, Catal. Commun. 7 (2006) 542.
[28] M. Mouaddib, V. Perrichon, M. Primet, J. Chem. Soc. Faraday Trans. 1 (85) (1989) 3413.
[29] J.A. Dalmon, P. Chaumette, C. Mirodatos, Catal. Today 15 (1992) 101.
[30] G.R. Sheffer, R.A. Jacobson, T.S. King, J. Catal. 116 (1989) 95.
[31] M. Blanchard, H. Derule, P. Canesson, Catal. Lett. 2 (1989) 319.
[32] J.E. Baker, R. Burch, S.J. Hibble, P.K. Loader, Appl. Catal. 65 (1990) 281.
[33] J.E. Baker, R. Burch, S.E. Golinski, Appl. Catal. 53 (1989) 279.
[34] N.D. Subramanian, G. Balaji, Challa S.S.R. Kumar, James J. Spivey, Catal. Today 147 (2009) 100.
[35] X. Xu, J.J.F. Scholten, D. Mausbeck, Appl. Catal. 81 (1992) 91.
[36] A.Y. Khodakov, A. Griboval-Constant, R. Bechara, V.L. Zholobenko, J. Catal. 206 (2002) 230.
[37] Ø. Borg, S. Eri, E.A. Blekkan, S. Storsæter, H. Wigum, E. Rytter, A. Holmen, J. Catal. 248 (2007) 89.
[38] A.Y. Khodakov, A. Griboval-Constant, R. Bechara, F. Villain, J. Phys. Chem. B 105 (2001) 9805.
[39] A. Griboval-Constant, A.Y. Khodakov, R. Bechara, V.L. Zholobenko, Stud. Surf. Sci. Catal. 144 (2002) 609.
[40] A.Y. Khodakov, R. Bechara, A. Griboval-Constant, Appl. Catal. A 254 (2003) 273.
[41] H. Karaca, O.V. Safonova, S. Chambrey, P. Fongarland, P. Roussel, A. Griboval-Constant, M. Lacroix, A.Y. Khodakov, J. Catal. 277 (2011) 14.
[42] H. Karaca, J. Hong, P. Fongarland, P. Roussel, A. Griboval-Constant, M. Lacroix, K. Hortmann, O.V. Safonova, A.Y. Khodakov, Chem. Commun. 46 (2010) 788.
[43] S. Deng, W. Chu, H. Xu, L. Shi, L. Huang, J. Nat. Gas Chem. 17 (2008) 369.
[44] P. Scherrer, Göttinger Nachrichten, 1918.;
R. Zsigmondy, Kolloidchemie, third ed., 1920, p. 394.
[45] B. Ravel, M. Newville, J. Synchrotron Rad. 12 (2005) 537.
[46] P.A. Chernavskii, A.Y. Khodakov, G.V. Pankina, J.-S. Girardon, E. Quinet, Appl. Catal. A 306 (2006) 108.
[47] P.A. Chernavskii, J.-A. Dalmon, N.S. Perov, A.Y. Khodakov, Oil Gas Sci. Technol. 64 (2009) 25.
[48] C. de Julián Fernandez, G. Mattei, C. Maurizio, E. Cattaruzza, S. Padovani, G. Battaglin, F. Gonella, F. D'Acapito, P. Mazzoldi, J. Magn. Magn. Mater. 290–291 (2005) 187.
[49] Z.Q. Yang, C.Y. You, L.L. He, J. Alloys Compd. 423 (2006) 128.
[50] H. Figiel, Ł. Gondek, B. Dubiel, F. Ciura, J. Chmist, A. Czyrska-Filemonowicz, J. Magn. Magn. Mater. 320 (2008) 2022.
[51] J.O. Lee, H.K. Kim, G.H. Kim, W. Y Jeung, J. Appl. Phys. 99 (2006) 55 (art. no. 08B704).
[52] H. Scott Fogler, Elements of Chemical Reaction Engineering, Prentice Hall PTR, Upper Saddle River, New Jersey, 1999.
[53] S. Chambrey, P. Fongarland, H. Karaca, S. Piché, A. Griboval-Constant, D. Schweich, F. Luck, S. Savin, A.Y. Khodakov, Catal. Today 171 (2011) 201.
[54] A. Jean-Marie, A. Griboval-Constant, A.Y. Khodakov, F. Diehl, C. R. Chim. 12 (2009) 660.
[55] P. Ganesan, H.K. Kuo, A. Saaverda, R.J. DeAngelis, J. Catal. 52 (1978) 319.
[56] X. Liu, C.T. Prewitt, Phys. Chem. Miner. 17 (1990) 168.
[57] K. Petrov, K. Krezhov, P. Konstantinov, J. Phys. Chem. Solids 50 (1989) 577.
[58] G.G. Volkova, T.M. Yurieva, L.M. Plyasova, M.I. Naumova, V.I. Zaikovskii, J. Mol. Catal. A 158 (2000) 389.
[59] J.-P. Bonnelle, J. Grimblot, A. D'huysser, J. Electron Spectr. 7 (1975) 151.
[60] D.G. Castner, P.R. Watson, I.Y. Chan, J. Phys. Chem. 93 (1989) 3188.
[61] V. Massarotti, D. Capsoni, M. Bini, A. Altomare and A.G.G. Moliterni Z. Zeitschrift fur Kristallographie 213 (1998) 259.
[62] S. Asbrink, L.J. Norrby, Acta Crystallogr. B 26 (1970) 8.
[63] W. Chu, P.A. Chernavskii, L. Gengembre, G.A. Pankina, P. Fongarland, A.Y. Khodakov, J. Catal. 252 (2007) 215.
[64] A. Jean-Marie, A. Griboval-Constant, A.Y. Khodakov, F. Diehl, Catal. Today 171 (2011) 180.
[65] S.I. Zabinsky, J.J. Rehr, A. Ankudinov, R.C. Albers, M.J. Eller, Phys. Rev. B. 52 (1995) 2995.
[66] A.Y. Khodakov, J. Lynch, D. Bazin, B. Rebours, N. Zanier, B. Moisson, P. Chaumette, J. Catal. 168 (1997) 16.
[67] G.P. Huffmann, N. Shah, J. Zhao, F.E. Huggins, T.E. Hoost, S. Halvorsen, J. Goodwin, J. Catal. 151 (1995) 17.
[68] I.J. Drake, K.L. Fujdala, S. Baxamusa, A.T. Bell, T. Don Tilley, J. Phys. Chem. B 108 (2004) 18421.
[69] G. Silversmit, H. Poelman, V. Balcaen, P.M. Heynderickx, M. Olea, S. Nikitenko, W. Bras, P.F. Smet, D. Poelman, R. De Gryse, M.-F. Reniers, G.B. Marin, J. Phys. Chem. Solids 70 (2009) 1274.
[70] W.M. Shaheen, A.A. Ali, Mater. Res. Bull. 36 (2001) 1703.
[71] D.G. Castner, P.R. Watson, I.Y. Chan, J. Phys. Chem. 94 (1990) 819.
[72] B. Ernst, A. Bensaddik, L. Hilaire, P. Chaumette, A. Kiennemann, Catal. Today 39 (1998) 329.
[73] R.M. Baillard-Letoumel, A.J. Gomez Cobo, C. Mirodatos, M. Primet, J.A. Dalmon, Catal. Lett. 2 (1989) 149.
[74] O. Ducreux, B. Rebours, J. Lynch, M. Roy-Auberger, D. Bazin, Oil Gas Sci. Technol. 64 (2009) 49.
[75] J. Häglund, A. Fernández Guillermet, G. Grimvall, M. Körling, Phys. Rev. B: Condens. Matter 48 (1993) 11685.
[76] C.R. Brundle, T.J. Chuang, D.W. Rice, Surf. Sci. 60 (1976) 286.
[77] M.C. Biesinger, L.W.M. Lau, A.R. Gerson, R.S.C. Smart, Appl. Surf. Sci. 257 (2010) 887.
[78] G.J. Kroes, Prog. Surf. Sci. 60 (1999) 1.
[79] A. Salin, J. Chem. Phys. 124 (2006) 104704.
[80] G.H. Guvelioglu, P. Ma, X. He, R.C. Forrey, H. Cheng, Phys. Rev. Lett. 94 (2005) 026103–026106.
[81] P. Chaumette, P. Courty, A. Kiennemann, R. Kieffer, S. Boujana, G.A. Martin, J.-A. Dalmon, P. Meriaudeau, C. Mirodatos, B. Hölhein, D. Mausbeck, A.J. Hubert, A. Germain, A. Noels, Ind. Eng. Chem. Res. 33 (1994) 1460.
[82] P. Courty, P. Chaumette, Natural Gas to Alcohols, NATO Workshop on Heterogeneous Catalysts for CO Conversion Nieuwport 17–22 April, 1988.
[83] D. Schanke, S. Vada, E.A. Blekkan, A.M. Hilmen, A. Hoff, A. Holmen, J. Catal. 156 (1995) 85.
[84] G. Prieto, A. Martínez, P. Concepción, R. Moreno-Tost, J. Catal. 266 (2009) 129.
[85] J.P. den Breejen, J.R.A. Sietsma, H. Friedrich, J.H. Bitter, K.P. de Jong, J. Catal. 270 (2010) 146.
[86] J.P. Den Breejen, P.B. Radstake, G.L. Bezemer, J.H. Bitter, V. Frøseth, A. Holmen, K.P. De Jong, J. Am. Chem. Soc. 131 (2009) 7197.
[87] F. Arena, K. Berbera, G. Italiano, G. Bonura, L. Spadara, F. Frusterri, J. Catal. 249 (2007) 185.
[88] M. Becker, R.N. D'Alnoncourt, K. Kähler, J. Sekulic, R.A. Fischer, M. Muhler, Chem. Vapor Depos. 16 (2010) 85.
[89] R. Yang, X. Yu, Y. Zhang, W. Li, N. Tsubaki, Fuel 87 (2008) 443.
[90] M.M. Günter, T. Ressler, B. Bems, C. Büscher, T. Genger, O. Hinrichsen, M. Muhler, R. Schlögl, Catal. Lett. 71 (2001) 37.
[91] T.B. Massals (Ed.), Binary Alloy Phase Diagrams, 2nd ed., ASM International, Materials Park, OH, 1990.
[92] A.S. Edelstein, V.G. Harris, D.R. Rolinson, L. Kurihara, Appl. Phys. Lett. 74 (1999) 3161.
[93] G. L Bezemer, J.H. Bitter, H.P.C.E. Kuipers, H. Oosterbeek, J.E. Holewijn, X. Xu, F. Kapteijn, A.J. van Dillen, K.P. de Jong, J. Am. Chem. Soc. 128 (2006) 3956.
[94] Ø. Borg, P.D.C. Dietzel, A.I. Spjelkavik, E.Z. Tveten, J.C. Walmsley, S. Diplas, S. Eri, A. Holmen, E. Rytter, J. Catal. 259 (2008) 161.